UNIVERSITY OF CALIFORNIA,
IRVINE

Nanocrystalline Al-Mg with Extreme Strength Due to Grain Boundary Doping

THESIS

submitted in satisfaction of the requirements
for the degree of

MASTER OF SCIENCE

in Mechanical and Aerospace Engineering

by

Chan Cheong (Simon) Pun

Thesis Committee:
Assistant Professor Timothy J. Rupert, Chair
Associate Professor Lorenzo Valdevit
Professor Emeritus Farghalli A. Mohamed

2016

TABLE OF CONTENTS

Page

LIST OF FIGURES

ACKNOWLEDGEMENTS

I would like to express my sincere gratitude to my thesis advisor and committee chair, Dr. Timothy Rupert for the immeasurable amount of support and guidance he has provided throughout this study. Dr. Rupert's wisdom and patient endurance throughout this project has been a blessing. Without his guidance and persistent help this thesis would not have been possible.

I would like to thank my committee members, Dr. Lorenzo Valdevit and Dr. Farghalli Mohamed, whose work in structural and mechanical behavior demonstrated to me the importance for and opportunities in mechanical properties of materials.

I thank all members of Nanoscale Mechanics and Materials Laboratory for intellectual and social support.

This study was supported by the U.S. Army Research Office under Grant W911NF-12-1-0511. Materials characterization was performed at the Laboratory for Electron and X-ray Instrumentation (LEXI) at UC Irvine, using instrumentation funded in part by the National Science Foundation Center for Chemistry at the Space-Time Limit (CHE-082913).

ABSTRACT OF THE THESIS

Nanocrystalline Al-Mg with extreme strength due to grain boundary doping

By

Chan Cheong (Simon) Pun

Master of Science in Mechanical and Aerospace Engineering

University of California, Irvine, 2016

Assistant Professor Timothy J. Rupert, Chair

A major difference between coarse-grained materials and nanocrystalline materials is the volume fraction of grain boundaries, which is the factor that alters nanocrystalline materials' physical and mechanical properties. Mechanical properties are also changed due to the fact that dislocation movements are impeded by small grains and other enhanced stabilizing mechanisms (dislocation locking, Zener pinning, etc.), reducing the driving force for deformation. The understanding of physical phenomena that takes place in such microscopic level poses an extremely interesting area of study where grain boundaries can be manipulated to alter physical and mechanical properties of a material. This thesis focuses on grain boundary doping as a mean of manipulation. Nanocrystalline Al and Al-Mg alloys with an average grain size of 24 nm were used to isolate the effect of grain boundary doping on strength. To begin, Mg was added to the Al lattice using mechanical milling, a process that produces materials in nanocrystalline form. This was followed by annealing treatments to induce segregation of solute (Mg) to the grain boundary, therefore changing the overall energy state that affects material properties. A combination of energy dispersive spectroscopy and X-ray diffraction were used to quantify the composition of the grain interiors and grain boundaries, then the relative contributions of solid solution strengthening and grain boundary segregation were extracted. Our results showed that nanocrystalline Al-7 at. % Mg had a maximum hardness of 4.56 GPa, approximately three times the hardness of pure nanocrystalline Al with the same grain size. Microcompression experiments on the strongest powder alloys indicated a yield strength value of 865 MPa and a specific strength value of 329 kN·m/kg, making these materials among the strongest Al alloys ever made. This work confirms that grain boundary segregation lowers the overall energy state and increases strength.

Chapter 1: Introduction

1.1 Background on Nanocrystalline Materials

Nanocrystalline materials are referred to as single- or multi-phase polycrystalline solids with a grain size below 100 nanometers. In having such small grain sizes, a nanocrystalline material is largely composed of interfaces, mainly grain boundaries and triple junctions. As a result, nanocrystalline materials present properties that are significantly different, and usually enhanced, from conventional coarse-grained materials. Materials that display microstructures in nano-dimension are sometimes referred to in the literature as nanocrystalline materials, nanocrystals, nanostructured materials, nanophase materials, nanometer-sized crystallites, or solids with nanometer-sized microstructural features. Nanocrystalline materials will be the appropriate term used in this study as the test specimens are solids made up of grains with nano-dimension.

There has been a tremendous emergence of research effort in nanocrystalline materials in the past 30 years. However, these materials are really not new and in fact, can be vastly found in nature. Many natural biological systems such as seashells and bones reveal nanostructured constituents formed chemically under ambient conditions [1]. Not only have these findings inspired the study of biomimetics and nanotechnology, but also have shown that material properties can be engineered and manipulated to meet new demands, specifically through changing grain size and boundary energy. Nanocrystalline metals exhibit useful mechanical properties such as high strength, prolonged fatigue life, and improved wear resistance [2-4]. Reducing a material's grain size results in an effective increase in the number of grain boundaries, which act as obstacles to dislocation motion [5]. For grain sizes from ~15-100 nm, plasticity is dominated by dislocations which are emitted from grain boundary sources, travel

across the grain while being momentarily pinned at the ends at boundary sites, and finally are absorbed into the opposite grain boundary [6]. While plasticity is still based on dislocation motion, the grain boundary is now heavily involved in the entire process and local grain boundary state should be important.

1.2 Grain Boundary Doping

1.2.1 Grain Boundary Relaxation

It has been reported that grain boundary relaxation, a low-temperature process where energy stored in the form of excess grain boundary dislocations is released as the boundary transforms to a more equilibrium configuration, enhances mechanical properties such as yield strength and hardness [7-9]. Aging and annealing experiments have been conducted on nanocrystalline specimens to show that materials that have experienced specific heat treatment gain atomic order in nonlattice sites (i.e., grain boundaries) [10]. This structural evolution corresponds to a strengthening effect and is understood in which relaxation at nonequilibrium boundaries serve as an alleviating mechanism to the excess boundary defects that could act as additional sources and sinks for dislocation glide or as facilitators of grain boundary sliding [11].

1.2.2 Thermal Stability

The energetic mechanism that dominates grain growth is controlled by a number of microstructural factors, which include second-phase particles, solute drag, pore drag, grain boundary energy, and ordering [12]. It is common to find kinetic mechanisms in the literature and commercially that metallic systems often contain second-phase particles that act as barriers to driving forces enabling grain boundary migration and grain growth. Second-phase particles

and drag elements inhibit grain growth through a process known as Zener pinning, where fine particulates reside in the grain boundaries and prevent migration by exerting pressure opposite to the driving forces [13]. Both images taken using bright field transmission electron microscopy (BF TEM) in Fig 1.1 show second-phase particles pinning grain boundaries and restricting grain boundary movement [13, 14]. Zener pinning therefore increases the activation energy for grain growth and allows a material to preserve fine grain size.

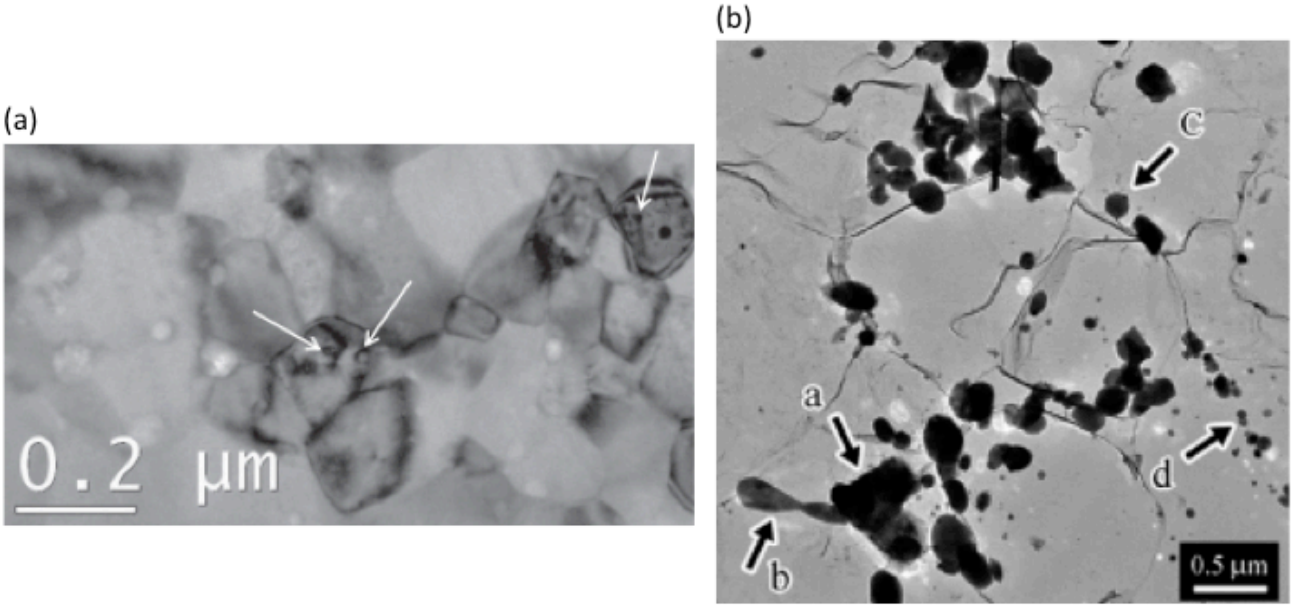

Fig. 1.1 BF TEM micrograph showing (a) TiN nanoparticles in cryomilled Ti matrix [13] and (b) four types of inert particles in a Ni-based alloy where they reside in and pin grain boundaries [14].

A second stabilization technique is one initiated by thermodynamic mechanisms, similar to grain boundary relaxation, where solute elements preferentially segregate out of solution to the grain boundaries and lower the overall energy of system. Segregating solute elements change the chemical ordering at the grain boundaries by establishing metastable equilibrium structures, which eliminate excess free energy driving force for grain growth [15].

Molecular dynamics simulations have confirmed such relaxation [8, 16, 17], while also providing evidence that reducing the grain boundary energy via solute doping increases strength

[18]. Vo et al. used a combined Monte Carlo/molecular dynamics simulation technique to predict that strengths near the theoretical limit could be achieved if boundaries are heavily doped [19-22]. Ozerinc et al. confirmed that boundary doping can significantly increase the strength of nanocrystalline metals using nanoindentation experiments on Cu and Cu-Nb films with different grain sizes [23]. However, there are no existing studies that report how on grain boundary dopants affect strength in a systemic fashion. In order to understand the effect of dopants on strength, it is necessary to quantify the magnitude of strengthening as a function of dopant concentration. In this project, we seek to isolate the effect of grain boundary segregation on nanocrystalline strength using experiments on Al-Mg alloys with a constant grain size. By keeping grain size constant, the strengthening contribution from grain size reduction is constant among all testing samples. This will allow us to explicitly quantify the effect of strengthening contribution from solid solution strengthening and grain boundary doping. The distribution of solute in the grain interior and grain boundary regions is extracted, and then used to measure the respective contributions of solid solution strengthening and grain boundary segregation. We find that boundary segregation has a much stronger effect on strength than solid solution effect, while also observing that alloys that are roughly three times as strong as pure nanocrystalline Al can be created through such methods. Microcompression experiments were used to confirm the extreme strength, showing that these alloys are among the strongest Al alloys that have ever been created.

Chapter 2 – Experimental Work

2.1 Alloying Element Selection

In many coarse-grained systems, the segregation of a second element to the grain boundary may be detrimental (ie. embrittlement, cold-cracking, etc.). A crack in a material can originate from hydrogen, oxide, or carbide particles accumulating at the grain boundaries and decrease cohesion to cause bond separation. However, segregating elements when introduced in nanocrystalline materials that lower grain boundary energy and act as a stabilization mechanism at the grain boundary may provide desirable mechanical effects. A particular challenge is in choosing the appropriate alloying element to best suit segregation and grain boundary stabilization. While Al was selected as the parent material, or solvent, by motivation to gain insight on lightweight systems, the alloying solute element must also be relatively lightweight to remain reasonable. Mg was highly desirable, owning a density of 1.74 g/cm^3 and is close to that of Al, which has a density of 2.70 g/cm^3. Mg was also a cost-effective candidate and ultimately chosen based on the work of Murdoch and Schuh [24], which suggested that Mg would have a positive enthalpy of segregation in Al and would therefore prefer to be at the grain boundaries. Fig. 2.1 shows an enthalpy map that outlines the segregation enthalpy of binary alloy systems, shedding light on material systems that are likely to experience grain boundary segregation.

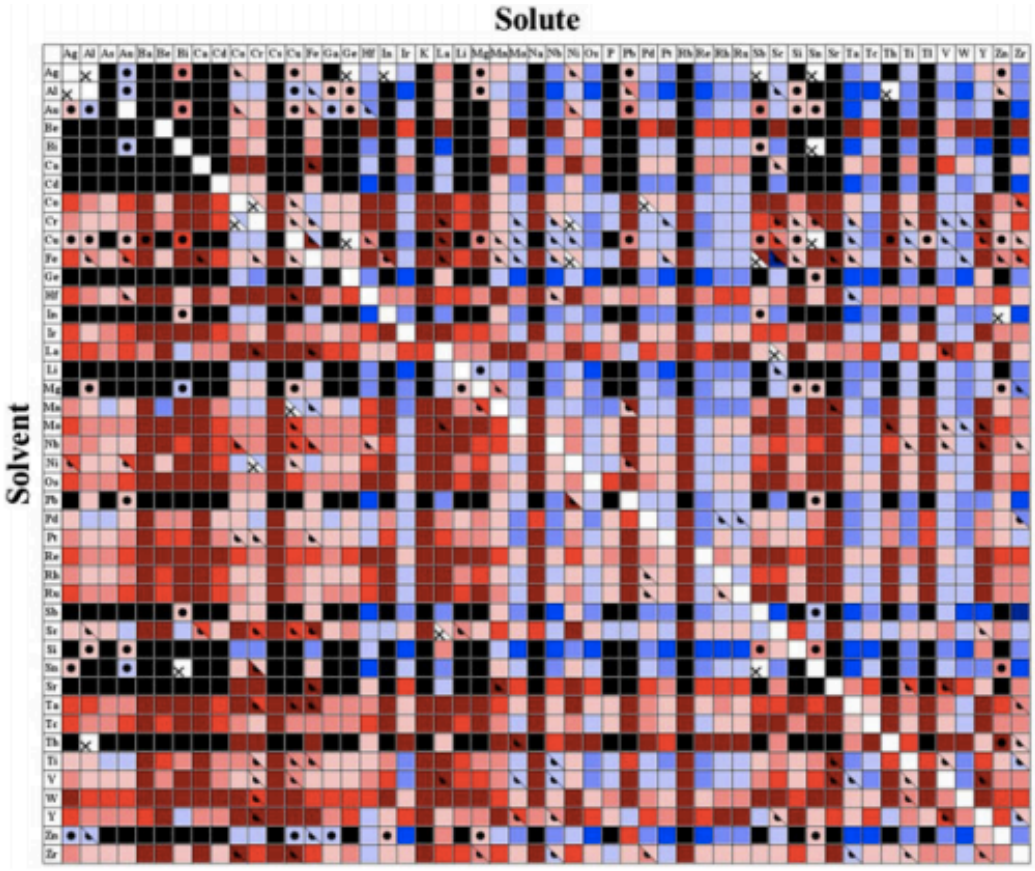

Fig. 2.1 Segregation enthalpy map for binary systems where red scale represents positive enthalpy or tendency of the solute to segregate to the grain boundary, blue scale represents negative enthalpy or antisegregation, black scale represents lack of data for calculation, a black dot represents non-Miedema or other data source, and a "x" represents sources not useful for segregation calculation [24].

2.2 Mechanical Alloying

Pure nanocrystalline Al and Al-Mg alloys with global Mg concentrations up to ~7 at.% were produced using a high-energy SPEX 8000M ball mill under Ar atmosphere at 2 x 10^{-3} torr. Mechanical alloying is a solid-state, high-energy powder processing technique that involves repeated welding, fracturing, and rewelding of powder particles in a ball mill. Fig. 2.2a shows a schematic of the deformation process during mechanical alloying, where the alloy material undergoes elastic, plastic, and shear deformation, and finally fractures. The condensed powder material then welds with others to become one large particle and the cycle repeats to further

reduce grain size. This process is capable of breaking a material, by exerting thermal and extreme kinetic energy, with coarse-grained microstructure to one with nanocrystalline microstructure. Studies have shown that a ball-to-powder ratio of 10 is most efficient to generate grain refinement effect [1]. Such best practice was adopted in the experiment, in other words, the weight of the stainless steel balls used to mill the metal powders were 10 times the weight of the total powder weight. Fig. 2.2b shows the SPEX Mill setup inside an Ar atmosphere chamber to prevent potential contamination and oxidation from air. 2.5 wt. % of stearic acid was used as milling lubrication agent, which prevents powder from welding to the ball mill during alloying. Furthermore, a study was carried out to evaluate the effect of milling time on grain size for Al-Mg alloys. Beyond 10 hours of milling, the grain sizes on all alloys remain roughly the same; thus, each alloy in this study was milled and compared after 10 hours.

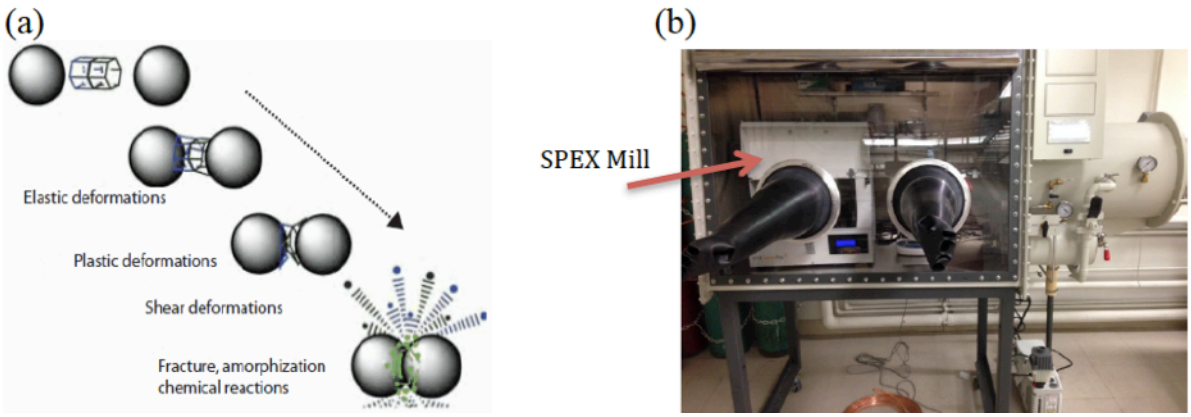

Fig. 2.2 (a) Schematic of material being mechanically alloyed (photo courtesy of Sigma Aldrich. Material Matters. Mechanochemical Effect [25]), where the material undergoes elastic, plastic, and shear deformation followed by fracture and eventually rewelding. (b) SPEX Mill 8000M is installed inside an Ar atmosphere fume hood to prevent oxidation and contamination.

2.3 Characterization

Selected samples were annealed at 150°C and 200°C under vacuum for 1 hour, to induce dopant segregation to the interfaces. Structural characterization of both as-milled and annealed

specimens was performed by using X-ray diffraction (XRD) in a Rigaku Ultima III Diffractometer with a Cu Kα radiation source operated at 40 kV and 30 mA. Fig. 2.3 shows machine setup in the Laboratory for Electron and X-ray Instrumentation at UCI. XRD profiles were used to verify that all alloys were polycrystalline, face-centered cubic (fcc) solid solutions. Scherrers equation was used to fit each profile peak in all samples, and then taking the average to estimate the alloy's grain size [26]. These XRD measurements indicate constant grain size and strain broadening among the alloys. Since coherent X-ray scattering only comes from the grain interiors, peak positions were used to quantify the distribution of solutes, which will be described in detail later. Energy dispersive spectroscopy (EDS) was performed on a Philips XL-30 field emission scanning electron microscope (SEM) at 10 kV to measure global alloy composition.

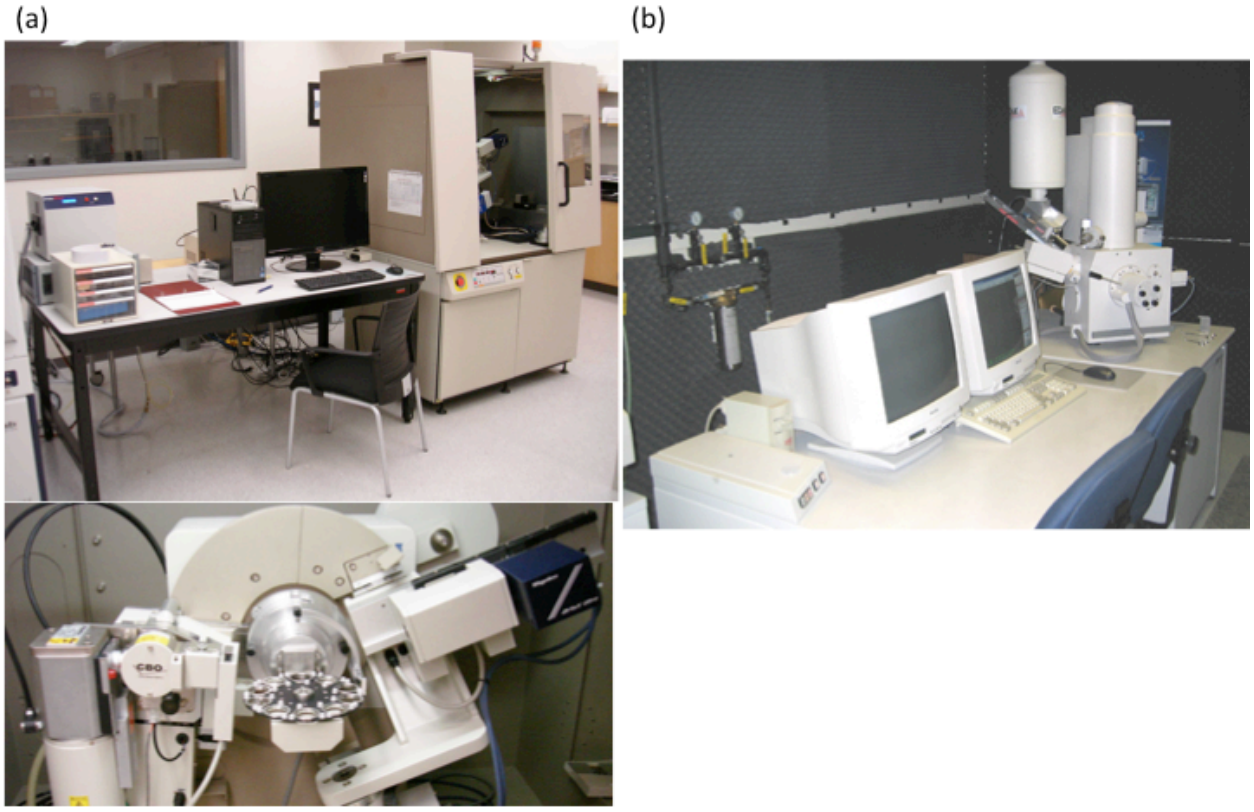

Fig. 2.3 Photo courtesy of Laboratory for Electron and X-ray Instrumentation at UCI [27] showing (a) X-ray diffraction station and (b) scanning electron microscopy station.

2.4 Nanoindentation and Microcompression

Hardness was measured using an Agilent G200 nanoindenter with a diamond Berkovich tip, which was calibrated with standard fused silica. The hardness values are based on 30 or more measurements per sample, with an indentation depth of 300 nm and a constant indentation strain rate of 0.05 1/s. Fig. 2.4a shows the main components of a nanoindenter and Fig. 2.4b shows the impression of the indenter head geometry. In the Agilent G200, hardness is defined as load applied to the test surface divided by the projected contact area, which is a function of the contact depth and indenter head geometry. During nanoindentation, the nanoindenter head will drive into the material, causing elastic and plastic deformation that leaves a residual impression on the sample. When the nanoindenter head is withdrawn, the elastic portion of the displacement is recovered in which enables calculations for elastic properties and hardness.

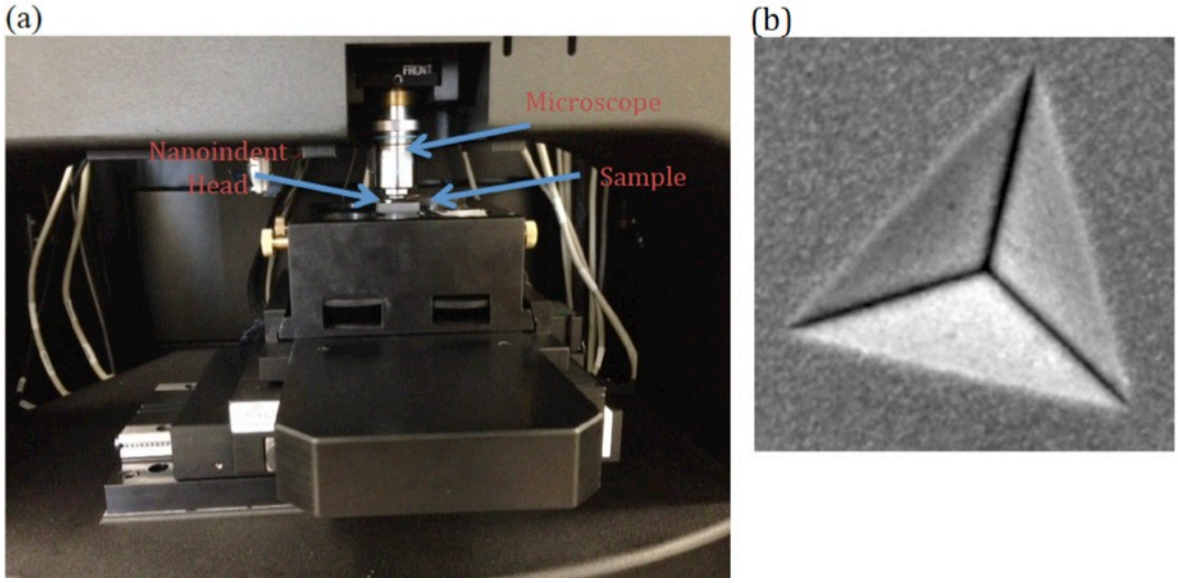

Fig. 2.4 (a) Photo shows three main components of an Agilent G200 nanoindenter: nanoindenter head, sample, and microscope. (b) Photo shows a residual impression of a Berkovich indenter [28].

Micropillars with average diameters of 6.3 μm and average heights of 16.4 μm were fabricated with automated lathe milling using focus ion beam (FIB), following the method of Uchic and Dimiduk [29]. The pillar aspect ratio (height/diameter) of ~2.5 was chosen to follow microcompression testing guidelines developed by Zhang et al. [30]. Fig. 2.5 shows images of micropillars in the top and side view. Yield strength was obtained by performing microcompression on three individual micropillars with a flat punch tip in the same nanoindenter, and then using the 0.7% yield strain offset criterion of Brandstetter et al. [31]

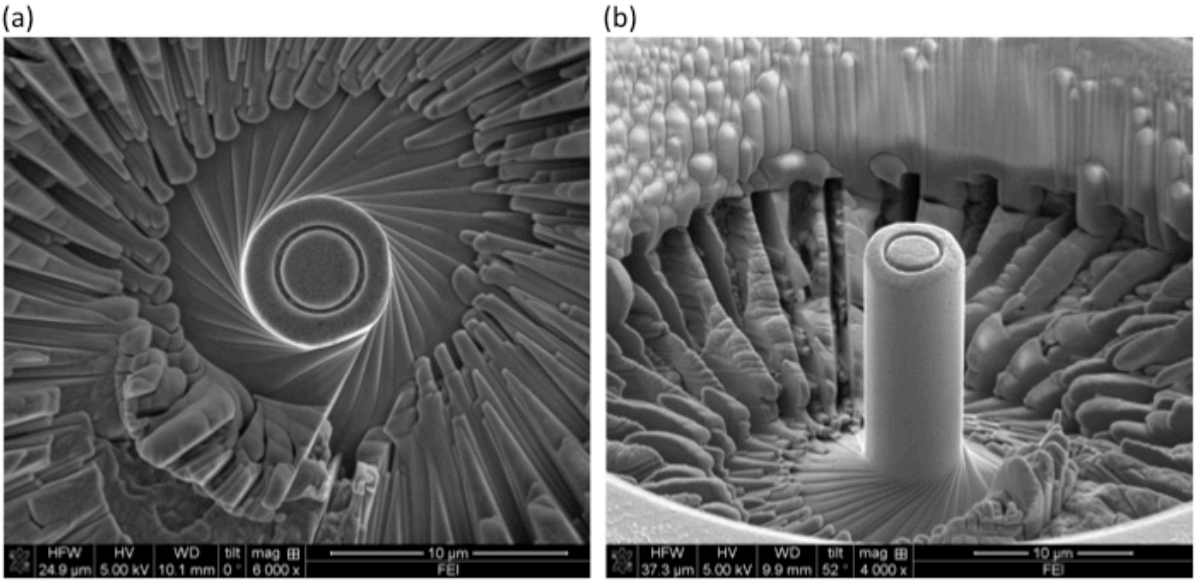

Fig. 2.5 SEM image of a pillar used for uniaxial microcompression testing in the (a) top view and (b) side view.

CHAPTER 3 – Results and Discussions

3.1 Alloy Strength

Alloys are mixture of metals that are usually created to reduce cost while keeping desirable properties of the parent material (ie. steel, brass, etc.). They can be produced in the form of solid solution, multi-phase, or intermetallic compounds. Generally speaking, alloys are referred to metallic compounds with superior mechanical properties such as yield strength and hardness. Superior mechanical properties can be achieved by slowing down or stopping dislocation movement until the stress is high enough to further propagate dislocations. Fig. 3.1 shows a demonstration of such concept, where various obstacles impede the movement of dislocation, requiring a higher flow stress to deform the material. Therefore, alloys that possess any type of obstacles would naturally experience an increase in strength and hardness. While that is true, a number of studies have reported that alloying could cause softening in solid solution [32, 33] and multi-phase [34] metallic compounds. In order to evaluate whether a specific alloy combination would result in strengthening, one must first understand the role of solutes during alloying. Moreover, one must understand the type of strengthening that occurs during alloying in order to accurately predict overall enhancement in mechanical properties.

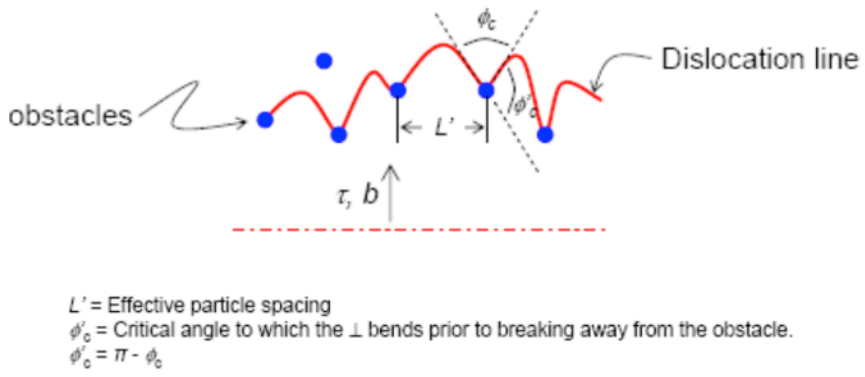

Fig. 3.1 Demonstration of obstacles impeding the movement of dislocations in a sample material [35].

3.1.1 Precipitation Hardening

Materials that result in multi-phase or second-phase after alloying are shown to experience strengthening known as precipitation hardening, where solutes evolve to become particulates, or obstacles, inside the parent material and impede the movement of dislocations throughout the matrix thus increasing overall strength. Two types of precipitation hardening are precipitation bowing and cutting, where the effect of one dominates the other once a critical particle size is reached [36]. Fig. 3.2 shows that as aging begins, the material is considered *underaged* where fine particulates start to form evenly throughout the material and force dislocations to cut through and overcome in a coherent manner, increasing the overall strain energy. As time continues, the material becomes *overaged* where the previous fine particulates begin to coarsen and interfere with dislocations in an incoherent manner, forcing dislocations to bow around particulates. Peak precipitation hardening is achieved when both fine and coarsened particulates are present in the material. Particulate size is a major contribution in the governing laws of precipitation hardening; however, surface energy, magnitude of Burgers vector, spacing between particulates, and the modulus of particulates are also important factors in determining material strength. While precipitation hardening was not observed in this study but only solid solution strengthening and grain boundary segregation were observed, the next sections will provide detailed explanation on their effects and mechanisms.

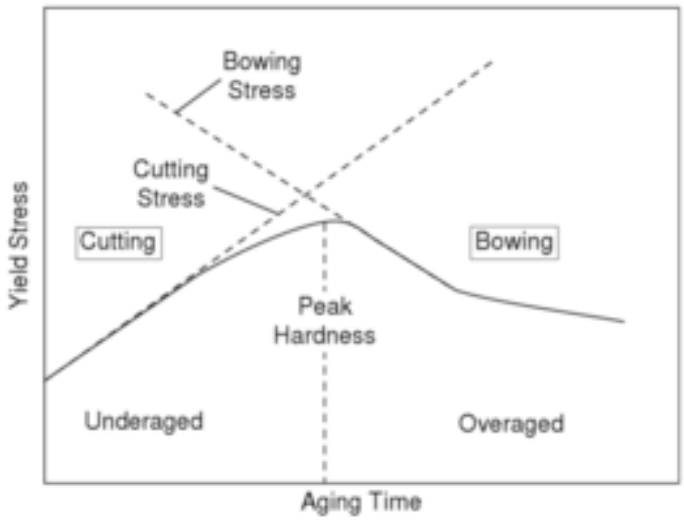

Fig. 3.2 Relative contributions of particle cutting and dislocation bowing [36].

3.1.2 Solid Solution Strengthening

Obstacles in solid solution are not as easy to imagine as those in precipitation hardening, where precipitates are the actual blockage for dislocation movement. In solid solution strengthening, solute atoms that go into solid solution with the parent material impose lattice strains on surrounding atoms, creating a lattice strain field that interfere with dislocation movement. Here the flow stress necessary to deform the material increases because additional driving force is now required to continue dislocation movement.

There are two types of solid solutions: substitutional and interstitial solid solution. Substitutional solid solution refers to a solute atom substituting a solvent atom in the crystal lattice. When the solute atom is bigger than that of the matrix, it is called big substitutional where compressive stress is imposed on surrounding atoms. When the solute atom is smaller than that of the matrix, it is called small substitutional where tensile stress is imposed on surrounding atoms [35]. Similarly in interstitial solid solution, a solute atom bigger than that of the matrix generates tensile stress on surrounding atoms; and a smaller solute atom generates

compressive stress on surrounding atoms. Shear stress is also applied on all strained atoms. Fig. 3.3 provides a graphical demonstration of each type of solid solution. In each of the cases, a strain field ultimately is created to cancel out strain caused from dislocations thus reduce the elastic strain energy of the system.

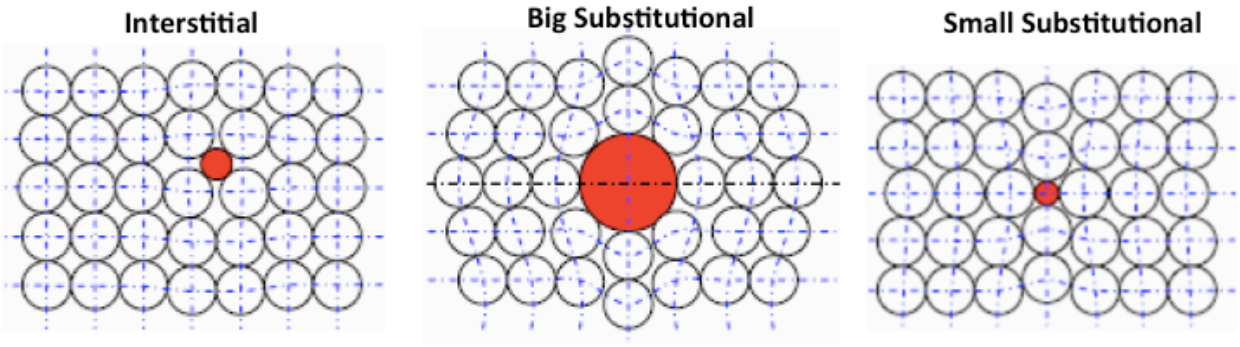

Fig. 3.3 Graphical demonstration of different types of solid solution [35].

3.1.3 Hardness as a Function of Alloy Composition

Fig. 3.4 presents hardness as a function of global alloy composition, showing that alloying dramatically increases the hardness of nanocrystalline Al-Mg. The hardness of pure nanocrystalline Al was measured to be 1.61 GPa. 1, 2, 5, and 7 at. % Mg were individually alloyed with balance Al, where strengthening effect decreases with solute addition. While 7 at. % Mg addition increases the hardness to 4.19 GPa, annealing the alloys leads to further hardening, with a maximum hardness of 4.56 GPa. This value is roughly three times as strong as pure nanocrystalline Al and is among the largest values that can be found in the literature, surpassing the hardness of commercial Al alloys [37]. XRD measurements gave a constant average grain size of 24 nm for all samples, meaning that neither doping or annealing altered the grain size and chemical effects alone (i.e., dopant distribution) were causing the strengthening.

To further develop this analysis, the relative contributions of solid solution strengthening and grain boundary segregation must be extracted, which requires knowledge of the composition in different parts of the microstructure. Eq. 1 summarizes the contributions to the overall hardness of the alloy:

$$H_{Alloy} = H_{Pure} + \Delta H_{Doping} \qquad (1)$$

where H_{Alloy} is the measured alloy hardness, H_{Pure} is the measured baseline nanocrystalline Al hardness, and ΔH_{Doping} is the solute doping contribution.

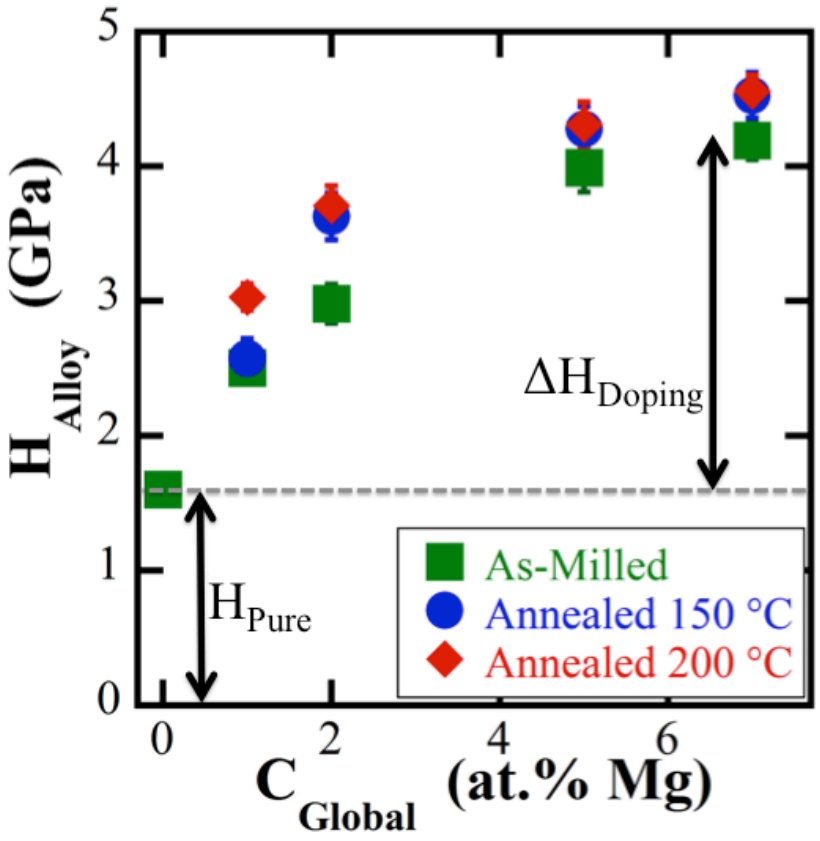

Fig. 3.4 Hardness values of Al-Mg alloys are plotted against the total amount of Mg solutes. While the as-milled alloys show high hardness, the annealing provides relaxation that further hardens the alloys. The dash line represents strengthening from grain size reduction, which is much less significant than that from grain boundary doping.

3.2 Deciphering of Strengthening Mechanisms

As discussed previously, Mg dopants can be incorporated either into the lattice as a solid solution or into the grain boundaries where both effects can be strengthening the alloy. Based on this circumstance, it is logical to break down ΔH_{Doping} to incorporate both solid solution and boundary doping effects, given in Eq. 2.

$$H_{Alloy} = H_{Pure} + \Delta H_{SSS} + \Delta H_{GB\ Seg.} \qquad (2)$$

where ΔH_{SS} is the total change in hardness from solid solution of a nanocrystalline alloy, and $\Delta H_{GB\ \ Seg.}$ is the total change in hardness from grain boundary doping.

In order to evaluate the strengthening effect from both mechanisms, the concentration of solutes at the grain interior as well as grain boundary must be individually extracted from the global composition. One method is to plot lattice parameter as a function of total composition to show how solute redistribution affects lattice size. Then, based on the difference between theoretical and experimental change in lattice size, we extract the amount of solutes in both grain interior and boundary. Fig. 3.5 shows that the lattice parameter of as-milled alloys follow the theoretical trend of Vegard's law up to 2 at. % Mg solute additions, then the lattice parameter deviates from the theoretical trend as additional solutes were added to lattice. Mg redistribution is confirmed by comparing XRD intensity profiles of pure Al and Al alloys. While some of the Mg continues to expand the lattice, those rejected can be located by understanding the origin of XRD signals, which are produced based on the crystallinity, or the ordered atomic planes, that are prevalent in the grain interior of a material. Grain boundaries, on the other hand, that are not crystalline in nature do not produce signals and are neglected in XRD profiles [38]. Therefore,

the remaining Mg atoms have simply segregated to the grain boundaries, lowering the overall energy and increasing grain boundary atomic ordering.

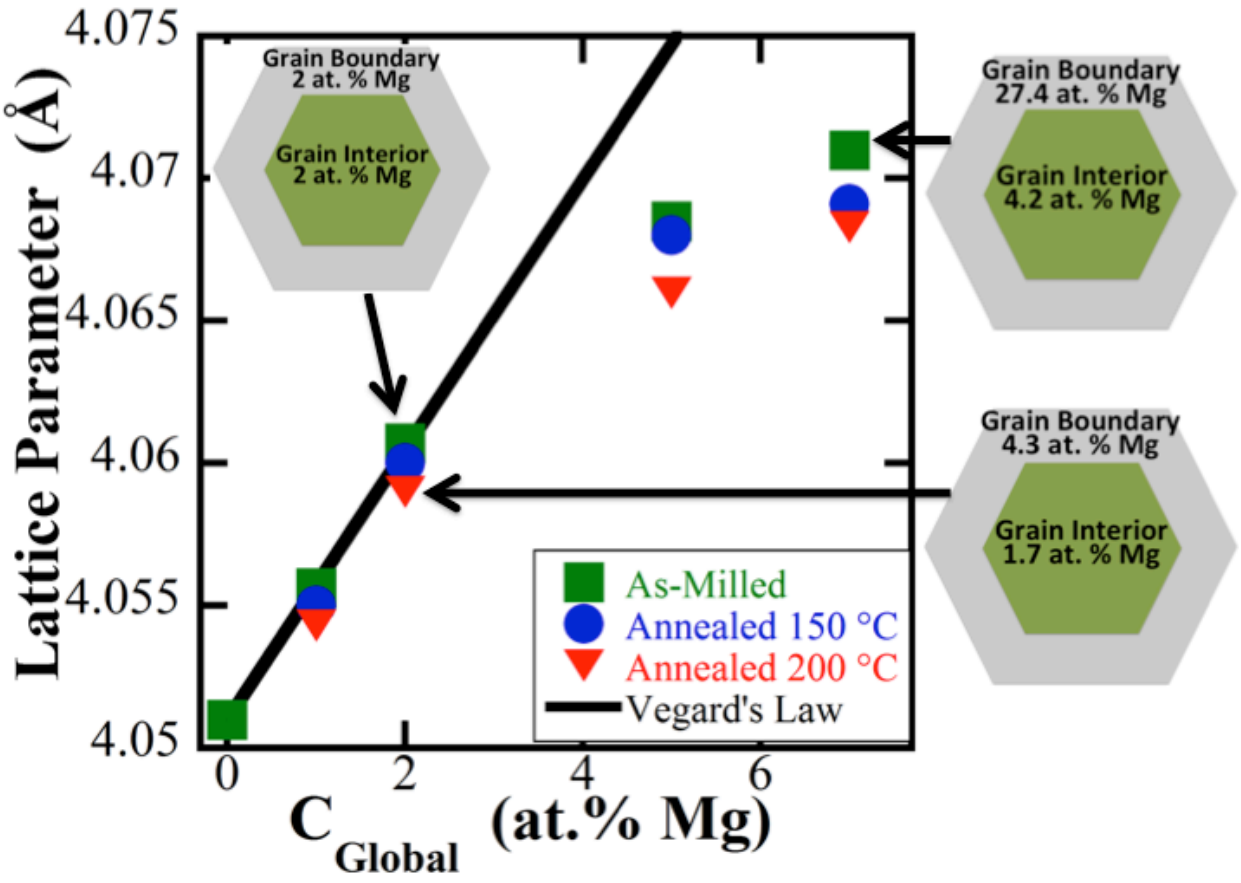

Fig. 3.5 Experimental data deviates from theoretical Vegard's law at solute concentration above 2 at. %, indicating grain boundary segregation. Mg atoms are observed to segregate out of lattice into the grain boundary as annealing temperature increases. Schematic of grain boundary doping depicts the grain interior region in green and boundary region in grey.

After annealing at 150°C and 200°C for 1 hour, a further reduction in lattice size is observed, which indicates further rejection of Mg out of the lattice and additional grain boundary segregation. This finding along with constant grain size confirms relaxation physics in which thermal energy from the annealing was spent reordering the grain boundary atoms to a more

ordered, equilibrium state. The schematic in Fig. 3.5 depicts the evolution of grain boundary doping, where the as-milled alloys containing Mg below 2 at. % initially have an even solute distribution at the grain interior and boundary. Mg can reach a saturation state that pushes additional solutes to the grain boundary, or undergo annealing that causes solutes to reside at the grain boundary.

3.2.1 Grain Boundary Segregation

Dopant concentration is calculated by analyzing the alloy system in having two components: grain boundaries and lattice as defined in Eq. 3.

$$C_{Global} = V_{GB}\, C_{GB} + V_{Lattice}\, C_{Lattice} \qquad (3)$$

where C_{Global} is the overall composition of the alloy, V_{GB} and C_{GB} are the volume fraction and composition of grain boundaries, respectively, and $V_{Lattice}$ and $C_{Lattice}$ are volume fraction and composition of lattice, respectively. A geometric model that uses a fourteen-sided tetrakaidecahedron as grain shape and hexagonal prisms as grain boundary components whose edges were triple junctions was used to calculate volume fraction for an alloy with grain size of 24 nm and grain thickness of 1 nm [39]. Total grain boundary components, or V_{GB}, make up 12% of the total volume, which indicates 88% $V_{Lattice}$. $C_{Lattice}$ of the Al-Mg system is calculated by applying experimental lattice parameters of the alloy, Al, and Mg obtained using XRD in Vegard's law [40]. Values of $C_{Lattice}$ obtained for 1, 2, 5, and 7 at. % Mg – Al in the as-milled and heat treated conditions are then recorded for later calculation of solid solution strengthening contribution. Next we take the computed $C_{Lattice}$ values and apply to Eq. 3 where we can obtain C_{GB} to calculate strengthening contribution from grain boundary doping. This method allows for a direct study in the relationship between strength and dopant concentration.

A model that captures solid solution strengthening in nanocrystalline alloys was developed by Rupert et al. [33] and is displayed in Eq. 4.

$$\Delta\tau = \Delta\tau_{nc,SS} + \Delta\tau_{Fleischer} \qquad (4)$$

where $\Delta\tau$ is the shear strength of the alloy, $\Delta\tau_{nc,\,SS}$ is the shear strength of a nanocrystalline solid-solution alloy, and $\Delta\tau_{Fleischer}$ is the shear strength of a coarse-grained solid-solution alloy. The shear strength of a nanocrystalline solid-solution alloy, $\Delta\tau_{nc,SS}$, is presented in Eq. 5.

$$\Delta\tau_{nc,SS} = \frac{G_{solvent}\, b_{solvent}}{d} \cdot \left[\left(\frac{1}{G_{solvent}}\frac{\partial G}{\partial c} + \frac{1}{b_{solvent}}\frac{\partial b}{\partial c}\right)\cdot c + \left(\frac{1}{G_{solvent}}\frac{\partial G}{\partial c}\cdot\frac{1}{b_{solvent}}\frac{\partial b}{\partial c}\right)\cdot c^2\right] \qquad (5)$$

where $G_{solvent}$ is the shear modulus of the solvent element, $b_{solvent}$ is the Burgers vector of the crystal lattice in the solvent element, d is the average grain size of the alloy, and c is the composition of the solute element, or the equivalent of $C_{Lattice}$. The shear strength of a coarse-grained solid-solution alloy, $\Delta\tau_{Fleischer}$, is presented in Eq. 6.

$$\Delta\tau_{Fleischer} = A \cdot G_{solvent} \cdot \varepsilon_s^{3/2} \cdot c^{1/2} \qquad (6)$$

where A is equal to 0.021, a fitting parameter found from coarse-grained data [41] and ε_s is an interaction parameter. The shear strength obtained in Eq. 4 – 6 is multiplied by $\sqrt{3}$ according to the Von Mises criterion for converting shear strength to an equivalent uniaxial strength and is increased by a factor of 3.8 using Tabor's relation [42] to convert to hardness value. All $C_{Lattice}$ values are inserted into Eq. 5 to obtain solid solution strengthening contribution.

It is observed that solid solution strengthening only contributes to a small amount of alloy hardening, with the maximum impact of 800 MPa at 4.2 at. % Mg in solution. This strengthening amount is insufficient to explain the dramatic strength increase presented earlier in Fig. 3.4, which motivates the exploration of strengthening contribution that comes from grain boundary doping. Hardness contribution from grain boundary doping was obtained by subtracting out hardness values from solid solution and pure Al in the as-measured alloy

hardness values, seen in Fig 3.4. Fig. 3.6 shows hardness results as a function of solute composition in both lattice and in grain boundary, where Fig. 3.6a shows strengthening effect from solid solution and Fig. 3.6b shows strengthening effect from grain boundary doping in an increasing logarithmic form.

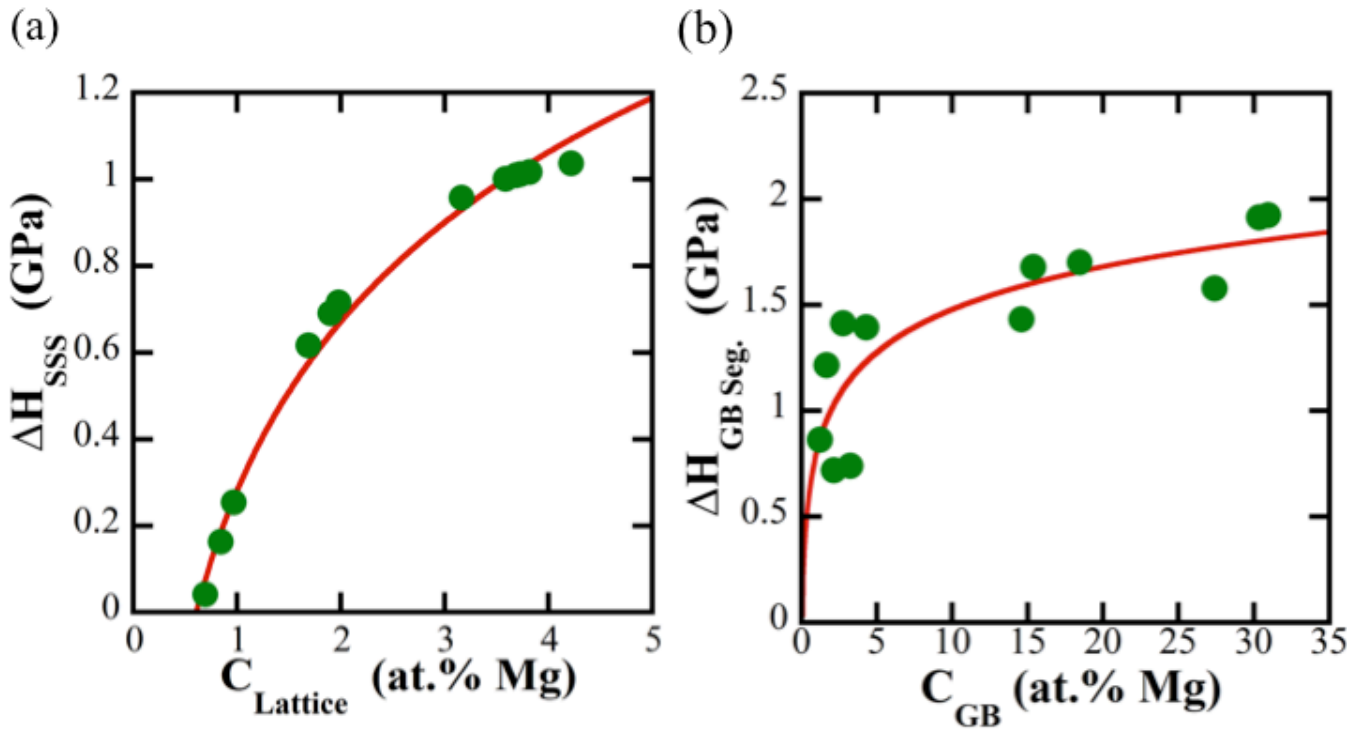

Fig. 3.6 Hardness plotted against Mg concentration in (a) lattice and (b) grain boundary. While there is strengthening effects from solid solution and grain size reduction, grain boundary doping offers major strengthening.

3.3 Grain Boundary Energy and Strengthening Effect

As seen in Fig. 3.6b, a concentration of 31 at. % Mg at the grain boundary greatly increases alloy hardness by 1.92 GPa. The strengthening factor and strengthening trend from grain boundary doping is comparable to those found in previous studies by Tucker et al. and Ozerinc et al. [18, 23]. Structurally ordered, equilibrium grain boundaries enhance yield strength

by means of decreasing interfacial excess free volume [7] and increasing the activation energy barriers required for dislocation nucleation [17]. In our study, Mg atoms are segregated to grain boundaries to add structural order, lower boundary energy, and as a result improve strength. It is essential to note that strengthening is most effective during early doping periods. We see the strengthening effect becomes less effective and begins to plateau as dopant concentration increases. The observed phenomenon is likely due to that high-energy sites at the grain boundary are particularly active and become the initial regions effectively compromised by dopants. In addition, the dopant strengthening effect can be guided by Gibbs free energy, where dopants lower the grain boundary energy in such a way that follows Gibbs energy potential when the system approaches equilibrium. This phenomenon is confirmed by various thermodynamic models found in the literature [43]. The grain boundary experiences *non-equilibrium segregation,* a term referred to the rate- and temperature-dependent segregation of solutes in which generally stops as time approaches infinity or when the grain boundary energy state reaches full equilibrium. The amount of segregation in a binary system can be related to grain boundary energy and total solute concentration by observing the Gibbs adsorption isotherm shown in Eq. 7,

$$\Gamma = -\frac{1}{R\,T}\left(\frac{\delta\sigma}{\delta \ln X}\right)_{P,T} \qquad (7)$$

where Γ is the adsorption of solutes to atoms in the grain boundary, R is the universal gas constant, T is temperature, σ is grain boundary energy, X is the solute concentration, and the subscript P,T represents constant pressure and temperature, respectively.

While solutes begin to segregate to the grain boundary and allow the system to approach equilibrium, the energy potential would experience a significant initial drop, and then continues to decrease at a constant rate. This drop in energy is reflected in Fig. 3.6 where the material

experiences significant strengthening in the beginning, but follows an asymptotically strengthening style. A theoretical Gibbs–McLean model suggested that zero grain boundary energy could be achieved in alloys with high segregation energy, where the grain boundary is in thermodynamic equilibrium with the presence of solute atoms [44] in which the theoretical strength can be reached. In order to confirm that our findings agree with both theoretical and experimental studies where enhanced yield strength is a result of lowering grain boundary energy, yield strength data from specimens must be obtained and compared with hardness results. Microcompression testing was performed to gather yield strength information.

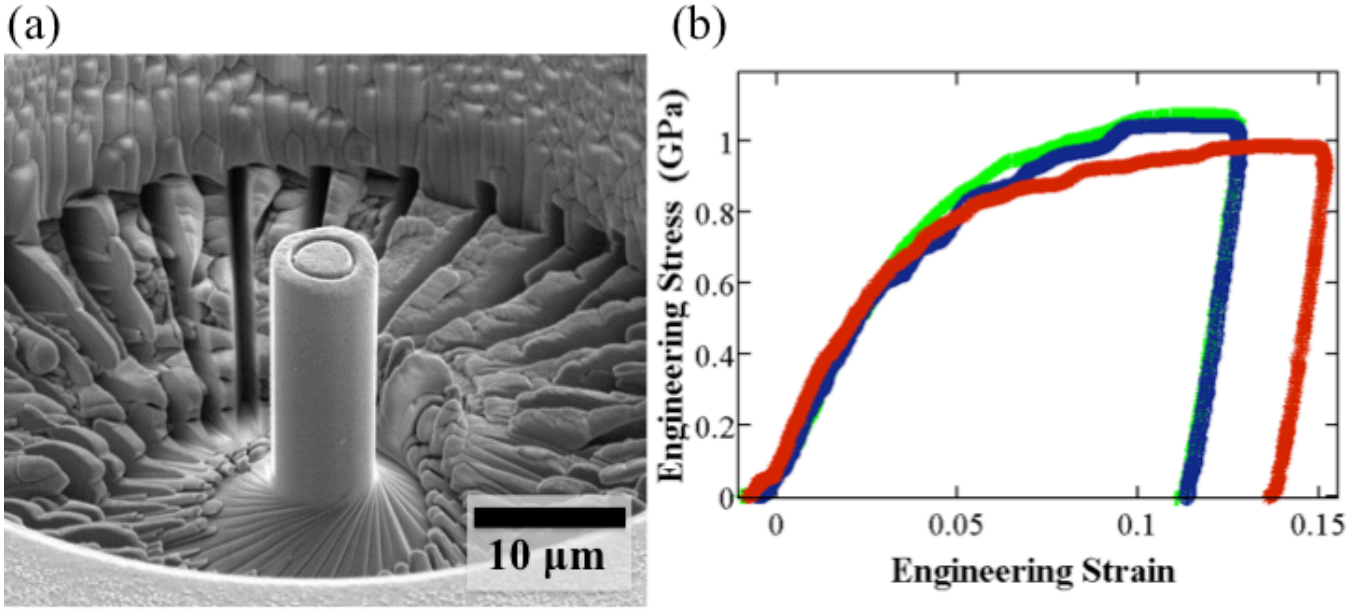

Fig. 3.7 (a) SEM image of a representative taper-free, as-prepared Al – 7 at. % Mg micropillar during uniaxial microcompression testing. (b) Stress-strain curves obtained from microcompression testing of three individual micropillars.

Fig. 3.7 shows microcompression testing results of our hardest alloy, where Fig. 3.7a shows SEM image of a representative taper-free, as-prepared micropillar during yield strength testing. Fig. 3.7b shows the stress-strain curves obtained by plastically deforming three

individual micropillars in uniaxial loading, where average yield strength of 865 ± 39 MPa was measured. Our alloy's yield strength is among the highest observed values in present published data for Al systems, with a specific strength of 329 kN·m/kg. In our experiment Al is strengthened by grain size reduction, solid solution, and grain boundary doping using Mg. A search in literature shows that strongest Al alloy uses 12 at. % Cr as a solute and has yield strength of 1104 ± 30 MPa with specific strength of 275 kN·m/kg, where strengthening effects are produced by grain size reduction, solid solution, and precipitation hardening [45]. While our alloy has a lower yield strength value, it weighs less than the Al-Cr alloy thus having a higher specific strength and puts this alloy among the strongest lightweight alloys ever made.

CHAPTER 4: Summary and Future Work

In conclusion, the strengthening effect from grain boundary doping is isolated and systematically studied in Al-Mg nanocrystalline alloys. Grain boundary dopant concentration can significantly increase hardness and yield strength by lowering boundary energy state. We observed Mg atoms segregate to the boundary when the Al lattice becomes oversaturated and when the alloy is annealed. We found that Mg dopants in the boundary of Al do not only improve strength, but also enhances thermal stability and obeys the scaling law guided by Gibbs free energy model. This observation agrees with other experimental and simulation studies [6, 16, 17, 23]. Decreasing the grain boundary energy increases the strength of the alloy system by virtue of enhancement in restricting dislocation movement and stabilization of grain boundary migration, both kinetically and thermally [18, 19, 22]. Using Mg dopants to lower grain boundary energy in a nanocrystalline Al -7 at. % Mg system, the alloy experiences an all-time high hardness value of 4.56 GPa, yield strength of 865 MPa, and specific strength of 329 kN·m/kg. In comparison with the Al -12 at. % Cr system, our alloy requires less dopant to create high strength and can better preserve the structural integrity of the Al lattice. The present experimental results provide great evidence that extreme strength can be achieved in nanocrystalline alloys by grain boundary doping.

Several opportunities to expand the work of this thesis could be, first, modeling this experiment using molecular dynamic (MD) to further investigate segregation phenomenon, and ask the question whether grain orientation has an effect on solute segregation rate and physics. A recent study has shown that manipulation of grain orientation and change of boundary chemistry can enhance yield strength and restrain intergranular cracks [46]; however, there was not an effort to relate the grain boundary energy state to preferred grain orientation. It would be

scientifically intriguing to discover the underlying relationship and improve our knowledge in solute segregation physics.

Second, develop nanocrystalline alloy using other syntheses such as electrodeposition or inert gas condensation, which are techniques that do not introduce the level of microstrain that mechanical alloying would on a material. While some of the thermal energy from annealing was spent on relieving the microstrain in the milled alloy, it would be interesting to discover whether more segregation would have occurred had the material contain less microstrain. These studies would allow further understanding of grain boundary segregation restrictions and enhanced doping results.

Finally, it would be beneficial for an engineer to explore the environmental variables such as annealing temperature and time on segregation rate and strength stability. A successful engineering design would take into account the material behavior during prolonged exposure in its operating and storing environment. Understanding the material characteristics can allow improved design and prevent failures.

REFERNCES

[1] C. Suryanarayana, Prog. Mater. Sci. 46 (2001) 1-184.
[2] K.S. Kumar, H. Van Swygenhoven, S. Suresh, Acta Mater. 51 (2003) 5743-5774.
[3] H.A. Padilla, B.L. Boyce, Exp. Mech. 50 (2010) 5-23.
[4] D.H. Jeong, F. Gonzalez, G. Palumbo, K.T. Aust, U. Erb, Scr. Mater. 44 (2001) 493-499.
[5] H. Gleiter, Prog. Mater. Sci. 33 (1989) 223-315.
[6] J.R. Weertman, Mechanical Behavior of Nanocrystalline Metals, in: C.C. Koch (Eds.), Nanostructured Materials – Processing, Properties, and Applications, William Andrew, NY, 2001, p. 537-565.
[7] D. Jang, M. Atzmon, J. Appl. Phys. 99 (2006) 083504.
[8] A. Hasnaoui, H.Van Swygenhoven, P.M. Derlet, Acta Mater. 50 (2002) 3927-3939.
[9] A.J. Detor, C.A. Schuh, J. Mater. Res. 22 (2007) 3233-3248.
[10] J. Loffler, J. Weissmuller, Phys. Rev. B. 52 (1995) 10.
[11] T.J. Rupert, J.T. Trelewicz, C.A. Schuh, J. Mater. Res. 27 (2012) 1285-1294.
[12] Y. Xun, E. Lavernia, F.A. Mohamed, Mater. Sci. Eng. A. 371 (2004) 135-140.
[13] S.S. Dheda, C. Melnyk, F.A. Mohamed, Mater. Sci. Eng. A. 584 (2013) 88-96.
[14] K. Song, M. Aindow, Mater. Sci. Eng. A. 479 (2008) 365-372.
[15] M. Saber, C.C. Koch, R.O. Scattergood. Mater. Res. Lette. 3 (2015) 65-75.
[16] N.Q. Vo, R.S. Averback, P. Bellon, A. Caro, Phys. Rev. B. 78 (2008) 241402.
[17] N.Q. Vo, R.S. Averback, P. Bellon, A. Caro, Scr. Mater. 61 (2009) 76-79.
[18] G.J. Tucker, D.L. McDowell, Inter. J. Plast. 27 (2011) 841-857.
[19] N.Q. Vo, J. Schafer, R.S. Averback, K. Albe, Y. Ashkenazy, P. Bellon, Scr. Mater. 65 (2011) 660-663.
[20] H.A. Murdoch, C.A. Schuh, Acta Mater. 61 (2013) 2121-2132.
[21] J. Weissmuller, Nanostruct. Mater. 3 (1993) 261-272.
[22] C.E. Krill, H. Ehrhardt, R. Birringer, Z. Metallk. 96 (2005) 1134-1141.
[23] S. Ozerinc, Tai, N. Vo, P. Bellon, R.S. Averback, W.P. King, Scr. Mater. 67 (2012) 720-723.
[24] H.A. Murdoch, C.A. Schuh, J. Mater. Res. 28 (2013) 2154-2163.
[25] Sigma Aldrich. Mater. Matters. 5 (2014) Fig. 6.
[26] Z. Zhang, F. Zhou, E.J. Lavernia, Metall. Mater. Trans. A 34 (2003) 1349-1355.
[27] Laboratory for Electron and X-ray Instrumentation. UC Irvine. 2016.
[28] Agilent Technologies. Nano Indenter G200 (2013) 7-28.
[29] M.D. Uchic, D.M. Dimiduk, Mater. Sci. Eng. A 400 (2005) 268-278.
[30] H. Zhang, B.E. Schuster, Q. Wei, K.T. Ramesh, Scr. Mater. 54 (2006) 181-186.
[31] C. Brandl, T.C. Germann, A. Misra, Acta Mater. 61 (2013) 3600.
[32] T.J. Rupert, Scr. Mater. 81 (2014) 44-47.
[33] T.J. Rupert, J.C. Trenkle, C.A. Schuh, Acta Mater. 59 (2011) 1619-1631.
[34] N. Takata, H. Ghassemi-Armaki, M. Takeyama, S. Kumar, Intermetal. 70 (2016) 7-16.
[35] L.M. Brown, R.K. Ham, in: A. Kelly, R.B. Nicholson (Eds), Strengthening Mechanisms in Crystals, Wiley, NY, 1971, p. 9-70.
[36] F.C. Campbell, Elements of Metallurgy and Engineering Alloys in: F.C. Campbell (Eds.), ASM International, OH, 1998, p. 139.

[37] J.R. Davis, Properties of Aluminum and Aluminum Alloys, in: J.R. Davis (Eds.), Aluminum and Aluminum Alloys, ASM International, OH, 1993, p. 579-706.
[38] C. Hammond, The Diffraction of X-rays, in: C. Hammond (Eds.), The Basics of Crystallography and Diffraction, Oxford University Press, Oxford, 2009, p. 203-240.
[39] G. Palumbo, S.J. Thorpe, K.T. Aust, Scr. Mater. 24 (1990) 1347-1350.Opin. Solid State Mater. Sci. 18 (2014) 253-261.
[40] A.R. Denton, N.W. Ashcroft, Phys. Rev. A. 43 (1991) 3161.
[41] B.H. Lee, S.H. Kim, J.H. Park, H.W. Kim, J.C. Lee, Mater. Sci. Eng. A 657 (2016) 115-122.
[42] F. Dalla Torre, H. Van Swygenhoven, M. Victoria, Acta Mater. 50 (2002) 3957-3970.
[43] P. Lejcek, Grain Boundary Segregation in: R. Hull, C. Jagadish, R.M. Osgood, Jr, J. Parisi, Z. Wang, H. Warlimont, Springer Series in Material Science, Springer, NY, 2010, p. 51.
[44] F. Liu, R. Kirchheim, J. Crys. Growth 264 (2004) 385-391.
[45] R.K. Gupta, D. Fabijanic, T. Dorin, Y. Qiu, J.T. Wang, N. Birbilis, Mater. Des. 84 (2015) 270-276.
[46] H. Fu, S. Song, L. Zhuo, Z. Zhang, J. Xie. Mater. Sci. Eng. A. 650 (2016) 218-224.